Multiparameter MR Imaging in the *6-OPRI* Variant of Inherited Prion Disease

E. De Vita, G.R. Ridgway, R.I. Scahill, D. Caine, P. Rudge, T.A. Yousry, S. Mead, J. Collinge, H.R. Jäger, J.S. Thornton, and H. Hyare

ABSTRACT

BACKGROUND AND PURPOSE: Inherited prion diseases represent over 15% of human prion cases and are a frequent cause of early onset dementia. The purpose of this study was to define the distribution of changes in cerebral volumetric and microstructural parenchymal tissues in a specific inherited human prion disease mutation combining VBM with VBA of cerebral MTR and MD.

MATERIALS AND METHODS: VBM and VBA of cerebral MTR and MD were performed in 16 healthy control participants and 9 patients with the *6-OPRI* mutation. An analysis of covariance consisting of diagnostic grouping with age and total intracranial volume as covariates was performed.

RESULTS: On VBM, there was a significant reduction in gray matter volume in patients compared with control participants in the basal ganglia, perisylvian cortex, lingual gyrus, and precuneus. Significant MTR reduction and MD increases were more anatomically extensive than volume differences on VBM in the same cortical areas, but MTR and MD changes were not seen in the basal ganglia.

CONCLUSIONS: Gray matter and WM changes were seen in brain areas associated with motor and cognitive functions known to be impaired in patients with the *6-OPRI* mutation. There were some differences in the anatomic distribution of MTR-VBA and MD-VBA changes compared with VBM, likely to reflect regional variations in the type and degree of the respective pathophysiologic substrates. Combined analysis of complementary multiparameter MR imaging data furthers our understanding of prion disease pathophysiology.

ABBREVIATIONS: IPD = inherited prion disease; MD = mean diffusivity; MTR = magnetization transfer ratio; VBA = voxel-based analysis; VBM = voxel-based morphometry

Human prion diseases are rapidly progressive, uniformly fatal neurodegenerative disorders[1] that can be inherited (IPD), occur sporadically, or be caused by iatrogenic or dietary infection. The discovery of variant Creutzfeldt-Jakob disease[2] has not been followed by a major epidemic; however, the existence of subclinical infections[3] and the evidence for secondary transmission by blood transfusion[4,5] reinforce the public health relevance of these conditions.

Most of the literature on prion disease imaging has focused on the acquired and sporadic forms rather than IPD. In prevalence studies, 15% of prion disease cases are IPD, a cause of early-onset dementia, with more than 30 different prion protein gene (*PRNP*) mutations identified.[6] The clinical phenotypes vary widely, with some mutations having a phenotype similar to sporadic Creutzfeldt-Jakob disease (eg, *E200K*), whereas others can mimic hereditary ataxias (eg, *P102L*) or Alzheimer disease (eg, some cases of *4-OPRI*).[7] The findings on conventional MR imaging are similarly variable.

In the United Kingdom, large kindreds presenting with 6 additional repeats in the octapeptide region (*6-OPRI* mutation), have been followed up for more than 2 decades with detailed reports of clinical symptoms[8] and neuropsychological features[9] but without systematic analysis of imaging findings. These pa-

Received September 17, 2012; accepted after revision December 11.

From the Lysholm Department of Neuroradiology (E.D., T.A.Y., H.R.J., J.S.T.) and National Prion Clinic (D.C., P.R., S.M., J.C., H.H.), National Hospital for Neurology and Neurosurgery, London, United Kingdom; and Neuroradiological Academic Unit, Department of Brain Repair and Rehabilitation (E.D., T.A.Y., H.R.J., J.S.T.), Dementia Research Centre (G.R.R.), Wellcome Trust Centre for Neuroimaging (G.R.R.), TRACK-HD (R.I.S.), and MRC Prion Unit, Department of Neurodegenerative Disease (D.C., P.R., S.M., J.C., H.H.), University College London Institute of Neurology, London, United Kingdom.

This study was supported by the UK Medical Research Council. Some of this work was undertaken at University College London Hospitals/University College London, which received a proportion of funding from the National Institute for Health Research Comprehensive Biomedical Research Centres funding scheme. The Dementia Research Centre is an Alzheimer's Research UK Coordinating Centre and has also received equipment funded by Alzheimer's Research United Kingdom. The Wellcome Trust Centre for Neuroimaging is supported by core funding from the Wellcome Trust 079866/Z/06/Z. TRACK-HD is funded by the CHDI Foundation, a not-for-profit organization dedicated to finding treatments for Huntington disease.

Please address correspondence to John Thornton, PhD, consultant clinical scientist (Magnetic Resonance Physics), University College London Hospitals NHS Foundation Trust, National Hospital for Neurology and Neurosurgery, Lysholm Department of Neuroradiology, Box 65, Queen Square, London WC1N 3BG; e-mail: john.thornton@ucl.ac.uk

http://dx.doi.org/10.3174/ajnr.A3504

tients characteristically present with frontoparietal dysfunction progressing for 7–15 years (mean, 11 years) that culminates in an akinetic mute state. Visuospatial, frontal executive, and nominal skills are significantly impaired in this patient group, and apraxia is an important early feature.

Brain atrophy has rarely been quantified in IPD, apart from a case report of a presymptomatic *P102L* gene carrier demonstrating early parietal atrophy[10] and a recent demonstration of parietal and occipital cortical thinning in patients with the *6-OPRI* mutation.[9] Quantitative MR imaging techniques such as MTR and MD mapping have revealed significant regional and whole-brain differences between patients with symptomatic prion disease and control participants.[11-14] However, these studies used region-of-interest or histogram analyses, possibly missing or diluting regionally specific changes.

VBA of structural images (VBM)[15] or MR imaging measures such as MD or MTR overcome these limitations because they do not require a priori anatomic hypotheses. These tools have not been applied in IPD, except for patients with the *E200K* mutation.[16-18]

We performed VBM, MTR-VBA, and MD-VBA in a cohort of patients with IPD who have the *6-OPRI* mutation, some of whom were previously studied with alternative methods.[12,13] We hypothesized that this multiparametric approach would localize brain abnormalities corresponding to known clinical symptoms and neuropsychological deficits and, further, that MTR and MD would quantify microstructural changes even in areas without significant volume loss on VBM.

MATERIALS AND METHODS

Patients

Patients attended the National Prion Clinic at the National Hospital for Neurology and Neurosurgery, London, United Kingdom, and were recruited into the UK MRC PRION-1 trial.[19] Ethical approval was granted by the Eastern Multicentre Research Ethics Committee, Cambridge, United Kingdom.

Full neurologic, Mini-Mental State Examination,[20] and Clinical Dementia Rating Scale sum of boxes=8[21] were recorded. Where several individual patient MR imaging datasets were available, the dataset acquired when the patient's Clinical Dementia Rating Scale was closest to the group median (Clinical Dementia Rating Scale=8) was selected. This approach allowed us to have a more homogeneous cohort and minimize the Clinical Dementia Rating Scale SD across the patient group.

Nine individuals with the *6-OPRI* mutation were studied (*6-OPRI* group: mean age, 38.1 ± 3.6 years; median Mini-Mental State Examination, 19 [range 11–27]; all codon 129MM). Sixteen healthy volunteers with no history of neurologic disorder were included (Controls group: mean age, 37.1 ± 10.7 years; all Mini-Mental State Examination, 30); Table 1.

Table 1: Patient demographics and clinical data

	Control Group	*6-OPRI* Group	*P* Value
N	16 (8 M)	9 (4 M)	–
Age (y)	37.1 ± 10.7	38.1 ± 3.6	ns
MMSE	30 (30–30)	19 (11–27)	<.001
CDR	–	8 (2–14)	.002[a]

Note:—CDR indicates Clinical Dementia Rating Scale; M, male; N, number; MMSE, Mini-Mental State Examination; ns, not significant ($P \geq 0.1$); *6-OPRI*, 6-octapeptide repeat insertion. Age values are mean ± SD. MMSE and CDR values are median (range).

[a] All comparisons were performed with the Mann-Whitney *U* test, except for CDR, for which the Wilcoxon test vs CDR = 0 was performed.

MR Imaging Acquisition

MR imaging was performed at 1.5T (GE Healthcare, Milwaukee, Wisconsin) by using the standard transmit/receive head coil. Sequences included the following:

1) Structural T1-weighted imaging (3D inversion recovery-spoiled gradient recalled-echo sequence [TR, 6.4 ms; TE, 14.5 ms; TI, 650 ms; flip angle, 15°; number of 1.5-mm partitions, 124; FOV, 24 × 18 cm^2; matrix, 256 × 192; total acquistion time, 9 minutes, 48 seconds]).
2) DWI with diffusion-weighting ("*b*") (single-shot echo-planar imaging [TR, 10 s; number of 5-mm sections, 30; FOV, 26 × 26 cm^2; matrix, 96 × 128]) with diffusion-weighting factors ("b-values") of 0 (B0) and 1000 s/mm^2 (b = 1000: TE, 101 ms; 1 average; acquistion time 1 minute, 20 seconds) and of 0 and 3000 s/mm^2 (b = 3000: TE, 136 ms; 3 averages; acquisition time 4 minutes) applied sequentially along 3 orthogonal axes. MD was calculated as:

$$MD_{1k,3k} = \ln(S_0/S_{1k,3k})/b_{1k,3k}{}^{22}$$

where S_0 and $S_{1k,3k}$ are respectively the local signal intensities of the B0 and mean of DWI (b = 1000 or b = 3000) acquired in 3 orthogonal directions (as only 3 gradient sensitization directions were used, this variable is actually an approximation of the mean diffusivity that could be measured with 6 or more directions).

3) MTR imaging (interleaved 2D, gradient-echo sequence, similar to the EuroMT sequence[23] [TR, 1500 ms; TE, 15.4 ms; flip angle, 70°; number of 5-mm sections, 30; FOV, 24 × 18 cm^2; matrix, 256 × 192; acquisition time 12 minutes]). Magnetization transfer presaturation was achieved with a Gaussian pulse of duration 12.8 ms and peak amplitude 23.2 μT giving a nominal bandwidth of 125 Hz, applied 2 kHz off water resonance. Scans with and without presaturation were interleaved for each TR period, ensuring exact coregistration of the pixels on saturated (Msat) and unsaturated (M0) images.[24] MTR was calculated from M0 and Msat images as MTR = (1–Msat/M0) × 100 in percentage units.
4) Fast spin-echo T2-weighted (TR, 6000 ms; TE, 106 ms; number of 5-mm sections, 22; FOV, 24 × 18 cm^2; matrix, 256 × 224; 2 averages) and FLAIR imaging (TR, 9897 ms; TE, 161 ms; TI, 2473 ms; number of 5-mm sections, 22; FOV, 24 × 24 cm^2; matrix, 256 × 224).

Imaging Analysis: Qualitative Analysis by Visual Inspection

The T2-weighted, FLAIR, and DWI images were reviewed independently (in an unblinded fashion) by 2 consultant neuroradiologists with experience in prion disease. Pathologic signal changes were assessed in the caudate, putamen, and thalamus and in the cortex of the frontal, parietal, temporal, and occipital lobes. When a discrepancy was identified, the images were re-reviewed

in a consensus reading and a κ statistic calculated to assess the level of agreement.

Imaging Analysis: Quantitative MR Imaging

VBM Spatial Preprocessing. Spatial processing for VBM was performed for structural data by using SPM8 (http://www.fil.ion.ucl.ac.uk/spm) as follows:

1) SPM8's "unified segmentation," combining segmentation, bias correction, and normalization to the Montreal Neurological Institute space into a single generative model (SPM "Segment").[25] The rigid normalization transformation component was used to produce approximately aligned images for the following step.
2) Generation of a cohort specific template for gray matter and WM segments by using the DARTEL toolbox in SPM8[26] using all participants.
3) Warping and resampling of individual gray matter and WM segments, normalizing them to the cohort-specific template. Local intensities for each voxel were modulated (ie, multiplied by the ratio of voxel volume before and after normalization) to account for normalization-associated volume changes.[27]

MTR-VBA Preprocessing. Rigid transformations between individual Msat images and corresponding T1 datasets were estimated and then combined with the warps computed for the T1 data to normalize individual MTR maps to the cohort VBM T1-template. As voxel MTR values are not directly related to voxel volume, data were not modulated.

MD-VBA Preprocessing. The MD ($b = 3000$ s/mm^2) dataset was rigidly aligned with the MD ($b = 1000$ s/mm^2) dataset (based on the corresponding B0 acquisitions). Affine transformations between MD and corresponding T1 images were estimated with the tool in NiftyReg (http://sourceforge.net/projects/niftyreg/)[28,29] to partially correct echo-planar imaging-associated geometric distortion (based on the MD ($b = 1000$ s/mm^2) B0 acquisitions). These transforms were then combined with the warps computed for the T1 data to normalize (with no modulation) individual MD ($b = 1000$ s/mm^2) and MD ($b = 3000$ s/mm^2) maps to the cohort VBM T1-template.

Statistical Analysis

An isotropic 6-mm full width at half maximum Gaussian kernel was applied to each of the 6 normalized datasets (gray matter, WM, MTR, MD ($b = 1000$ s/mm^2), and MD ($b = 3000$ s/mm^2)). An "objective" masking strategy[30] defined the voxels for subsequent statistical analysis on gray matter and WM segments separately; the resulting masks were combined for MTR and MD data analysis. For each dataset, the analysis involved an analysis of covariance consisting of diagnostic grouping (*6-OPRI* or controls) with individual age and total intracranial volume (estimated as the sum of gray matter, WM, and CSF segments) as covariates (using the same covariates for all analyses allowed for a more consistent model across modalities). Group differences between covariates were assessed with the 2-sample Mann-Whitney *U* test (PASW Statistics 18, SPSS, Chicago Illinois).

SPM-t maps ($P < .05$) after family-wise error multiple-comparison correction (with no cluster-extent threshold), and effect-size maps showing group differences as percentages of the control group mean were produced. We also computed the affine transformation between the DARTEL space (in which the SPM results were computed) and Montreal Neurological Institute space. Using these parameters, we also transformed the SPM maps and effect-size maps onto Montreal Neurological Institute space for visualization. Results are thus displayed in the Montreal Neurological Institute space overlaid on the average of the warped and smoothed T1 volumes. All are presented by using the neurologic convention (right hemisphere displayed on the right).

ROIs

To quantify differences in MR imaging measures, 3 ROIs were defined on the right hemisphere of the average warped and smoothed T1-volume, in the thalamus, head of the caudate, and putamen (ROI volume range, 0.59–0.60 mL). The ROIs were then verified for individual datasets to ensure that the smoothing had not introduced CSF contamination. The ROI mean from the corresponding warped and smoothed datasets for each patient was computed and between-group differences assessed by the 2-sample Mann-Whitney *U* test. To account for multiple comparisons over the 3 regions (but not the 4 metrics, as these tests are being compared with each other, rather than simply being searched over), $P < .01$ was considered significant.

RESULTS

Between controls and patients with *6-OPRI*, differences in age were not significant, in contrast to Mini-Mental State Examination and Clinical Dementia Rating Scale (Table 1). The total intracranial volumes were 1.42 ± 0.14 L (mean $\pm$ SD) in controls and 1.41 ± 0.20 L in patients with *6-OPRI* and were not significantly different.

Qualitative Analysis

On initial assessment, both raters agreed that there was no pathologic signal change in 7 of the 9 patients. There were discrepancies in 2 patients where DWI signal hyperintensity in the frontal cortex was noted in 1 patient and FLAIR signal hyperintensity in the perihabenular region noted in another patient (κ score, 0.835). On consensus review of these cases, it was decided that the findings were artifactual and that there was no evidence of pathologic signal change.

Quantitative Analysis

VBM. Within the supratentorial cortex, extensive bilateral symmetric gray matter volume reduction was seen in the perisylvian cortex: central opercular, insular cortex, middle and superior temporal gyri; parietal cortex: angular, supramarginal, and postcentral gyrus; and occipital cortex: lingual gyrus and cuneus. Less extensive gray matter reduction was also seen in the left superior frontal gyrus and cingulate gyrus. Within the deep gray nuclei, significant gray matter reduction was seen in the caudate and putamen bilaterally and within the posterior fossa; the cerebellar cortex bilaterally also showed significant gray matter reduction (Fig 1*A*).

The areas of significant WM reductions are more sparse and to a smaller extent. Significant areas of WM volume reduction in-

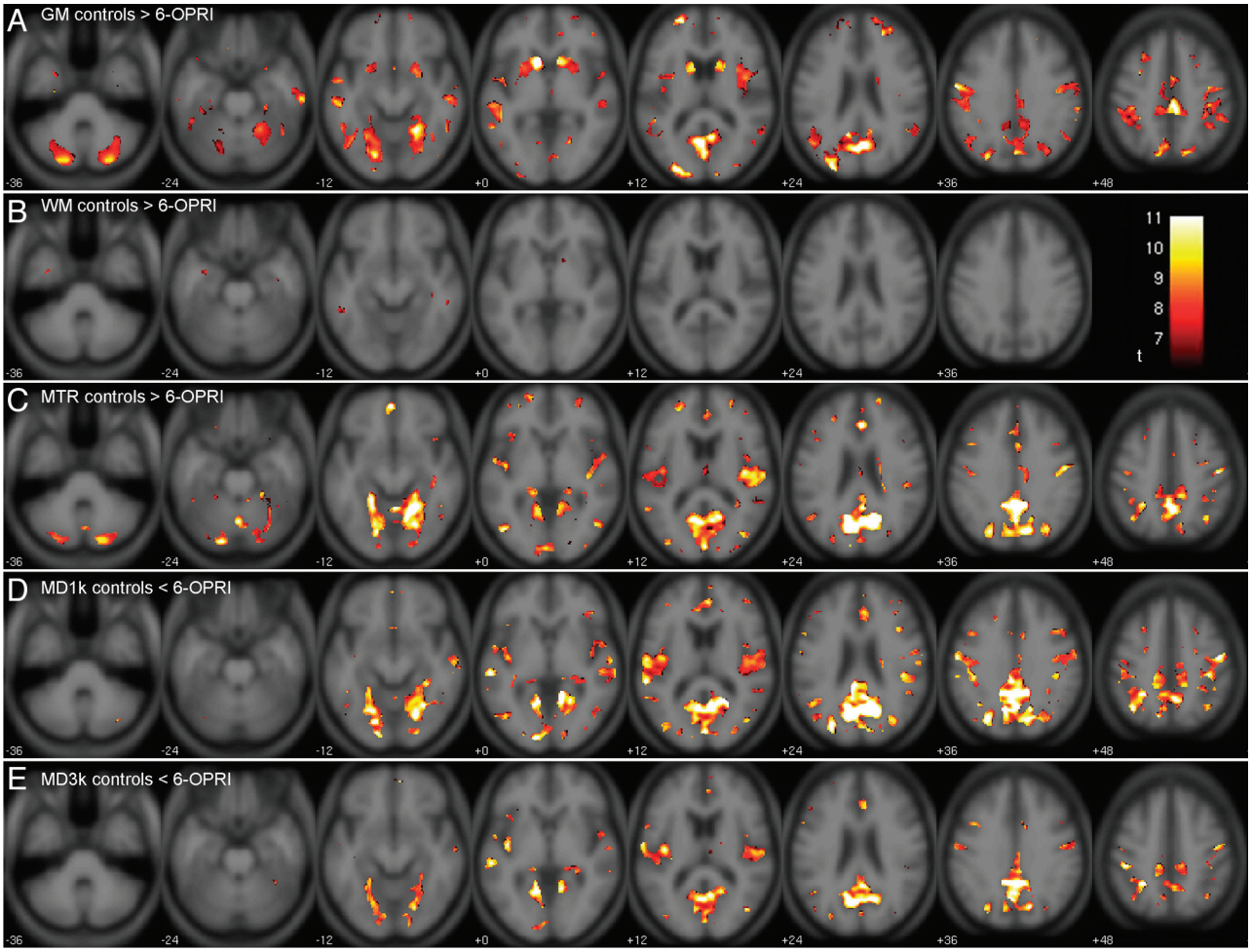

FIG 1. SPM-*t* maps for patients with the *6-OPRI* mutation compared with control participants. SPM-*t* maps showing significant differences between symptomatic patients with the *6-OPRI* mutation ($n = 9$) and healthy control participants ($n = 16$) for family-wise error $P < .05$. *A*, gray matter: controls >*6-OPRI*, $t \geq 6.60$. *B*, WM: controls >*6-OPRI*, $t \geq 6.07$. *C*, MTR: controls >*6-OPRI*, $t \geq 6.86$. *D*, MD (b = 1000 s/mm^2): controls <*6-OPRI*, $t \geq 7.03$. *E*, MD (b = 3000 s/mm^2): controls <*6-OPRI*, $t \geq 6.96$. The color bar represents the *t* value range.

Table 2: Significant clusters for WM VBM (Controls > *6-OPRI*)

k	Peak *P* Value (FWE corr)	Peak T	Peak Z	x	y	z	Description
175	<.001	10.59	6.16	−34	−4	−31	L temporal fusiform and parahippocampal gyri
176	.003	7.61	5.22	−52	−43	−3	L middle temporal gyrus
	.005	7.37	5.12	−56	−42	−12	L middle temporal gyrus
7	.017	6.66	4.83	−54	−29	−8	L middle temporal gyrus
6	.019	6.61	4.81	−39	−57	30	L angular gyrus
46	.006	7.25	5.08	−25	−31	−13	L hippocampus
45	.007	7.16	5.04	−26	−29	−8	L hippocampus and L parahippocampal gyrus
	.03	6.35	4.69	−20	−34	6	L thalamus
18	.035	6.27	4.66	−13	6	−3	L pallidum
97	.001	8.25	5.45	57	−35	−13	R middle temporal gyrus
	.017	6.67	4.83	49	−39	−9	R inferior temporal gyrus
	.018	6.66	4.83	47	−48	−11	R inferior temporal gyrus
148	.002	7.82	5.29	37	−12	−22	R temporal fusiform gyrus
	.003	7.72	5.26	37	−29	−13	R temporal fusiform gyrus
57	.009	7.01	4.98	26	−31	−6	R hippocampus
60	.012	6.86	4.92	13	8	−3	R pallidum
27	.004	7.58	5.21	2	−22	19	Midline-body of corpus callosum
3	.034	6.29	4.66	−5	−19	30	L body of corpus callosum
10	.022	6.54	4.78	5	−17	30	R body of corpus callosum

Note:—FWE corr indicates family-wise error corrected; L, left; MNI, Montreal Neurological Institute; R, right. k is the number of voxels within each cluster. All clusters of voxels above a voxel-level threshold FWE $P \leq .05$ of size $k > 2$ are shown. For the largest clusters, the table shows up to 3 local maxima more than 8 mm apart. The x, y, and z coordinates are in the MNI space. Peak-t and Peak-z values are within each cluster.

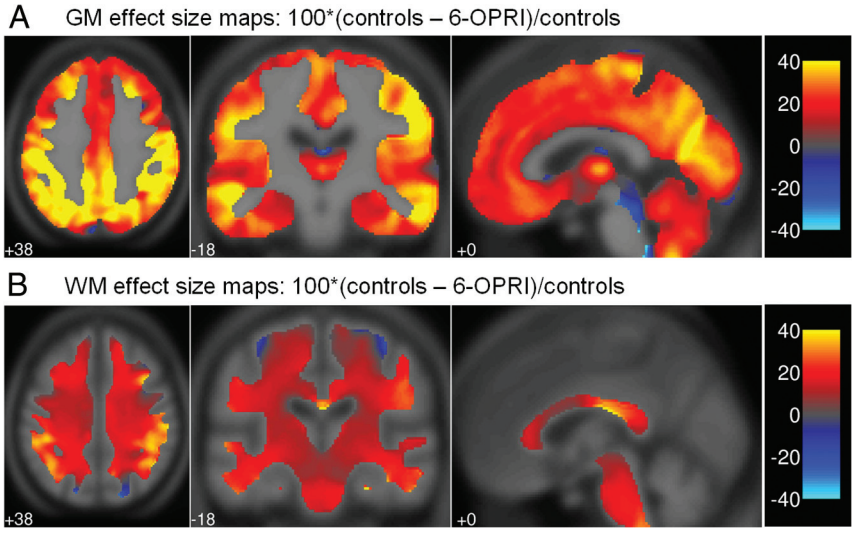

FIG 2. Effect size maps for all patients compared with control participants and patients with *6-OPRI* compared with control participants. Effect size maps demonstrating the percentage difference between patients with *6-OPRI* and controls in (*A*) gray matter volume and (*B*) WM volume calculated as 100*(controls-all patients)/controls displayed in the Montreal Neurological Institute space.

volved the anterior temporal lobes, the body of the corpus callosum, and hippocampus bilaterally (Fig 1*B*). A complete list of the coordinates and corresponding anatomic locations of the significant cluster peaks (for clusters with size $k > 2$) is presented in Table 2.

The effect maps (Fig 2*A*, 2*B*) demonstrated that the largest percentage differences were present in the insular cortex, middle and superior temporal gyri, angular and supramarginal gyri, lingual gyrus, and cuneus.

MTR. Significant MTR reductions in the *6-OPRI* group were topographically similar in the supratentorial cortex to those seen on VBM, with extensive involvement of the perisylvian regions, and parietal and occipital cortices bilaterally, as described above (Fig 1*C*). Within the deep gray nuclei, significant MTR reductions were seen in the posteromedial thalamus bilaterally only. In the posterior fossa, extensive involvement of the cerebellar cortex was seen.

Regarding the number of suprathreshold voxels, changes were more anatomically extensive on MTR-VBA than on VBM in the perisylvian regions, cuneus, and precuneus, where there is the impression of involvement of the subcortical WM, with significant reductions in the posteromedial thalamus, not seen on VBM. However, MTR-VBA did not detect significant MTR reductions in the caudate nucleus, putamen, or middle temporal gyri where VBM showed differences (Fig 1*C*).

MD. MD ($b = 1000$ s/mm^2). The largest clusters and most significant MD ($b = 1000$ s/mm^2) increases were seen in the gray matter and subcortical WM of the perisylvian, parietal, and occipital lobes (Fig 1*D*) and in the posteromedial thalamus bilaterally. Regarding the number of suprathreshold voxels, changes were more anatomically extensive on MD-VBA than on VBM, similar to MTR-VBA. No significant differences were seen in the cerebellar hemispheres (as seen on MTR) or in the basal ganglia (as seen on VBM).

MD ($b = 3000$ s/mm^2). Areas of significant MD ($b = 3000$ s/mm^2) increase overlapped those seen with MD ($b = 1000$ s/mm^2), although the extent and significance were generally smaller (Fig 1*D*,*E*). Reduced significance could arise from either reduced effect size (group difference) or increased variability. We investigated these influences by evaluating the non-normalized group difference, and a form of coefficient of variation given by the square root of the mean squared residuals (SPM ResMS Image) divided by the average of the 2 group means from the analysis of covariance model. Both the group difference and the coefficient of variation were larger for MD ($b = 1000$ s/mm^2) (data not shown), suggesting that the higher significance of MD ($b = 1000$ s/mm^2) changes is the result of a greater effect size than for MD ($b = 3000$ s/mm^2) and not simply a higher signal-to-noise ratio.

ROI Analysis

Mean values for patients with *6-OPRI* differed significantly from controls in all 3 ROIs for tissue-segment volumes, MTR, and MD ($b = 1000$ s/mm^2), and in the thalamic ROI only for MD ($b = 3000$ s/mm^2) (Table 3).

DISCUSSION

This systematic study is the first to describe the distribution of gray matter and WM volume changes and voxelwise MTR and MD changes in patients with IPD who have the *6-OPRI* mutation. We demonstrated anatomically specific mean tissue attenuation reduction in these patients that are consistent with previous qualitative reports. Using MTR and MD, we detected cortical and subcortical microstructural changes both coincident with and spatially independent of tissue volume changes. Some of these changes seem to be specific to the *6-OPRI* IPD mutation.

Local Volume Reductions Assessed with VBM

Brain atrophy occurs in all forms of prion disease,[8,31] but most reports are based on visual inspection rather than objective quantification. In an early case report, a presymptomatic *P102L* gene carrier demonstrated widespread supratentorial and cerebellar volume loss with relative sparing of the mesial temporal lobe structures.[11] In a recent study of patients with the *6-OPRI* mutation, significant cortical thinning was seen in the precuneus, inferior parietal cortex, supramarginal gyrus, and lingula.[9] Our study confirms these findings, with gray matter volume loss in such patients predominantly involving the perisylvian cortex, precuneus, and lingual gyrus and without significant involvement of the mesial temporal lobe structures.

These cortical changes relate well to clinical symptoms documented in patients with the *6-OPRI* mutation. Apraxia is an important early feature and is generally associated with lesions to the dominant parietal lobe and, specifically, the supramarginal gyrus. Visuoperceptual and visuospatial impairments known to be sensitive to right parietal damage are also common in this patient

Table 3: Mean values for tissue segment volumes, MTR, MD (b = 1000 s/mm^2), and MD (b = 3000 s/mm^2) in selected ROIs

Brain Region	Control Group	*6-OPRI* Group	*P* Value[b]
Right thalamus			
WM (tv)[a]	0.66 ± 0.07	0.57 ± 0.05	.002
MTR (%)	40.6 ± 1.2	38.9 ± 1.1	.002
MD1K ($\times 10^{-3}$mm^2/s)	0.81 ± 0.03	0.88 ± 0.05	<.001
MD3K ($\times 10^{-3}$mm^2/s)	0.63 ± 0.01	0.67 ± 0.03	<.001
Right caudate			
GM (tv)	0.74 ± 0.07	0.50 ± 0.08	<.001
MTR (%)	37.6 ± 1.1	33.8 ± 2.2	<.001
MD1K ($\times 10^{-3}$mm^2/s)	0.79 ± 0.03	0.88 ± 0.10	.001
MD3K ($\times 10^{-3}$mm^2/s)	0.63 ± 0.02	0.64 ± 0.03	NS
Right putamen			
GM (tv)	0.92 ± 0.12	0.60 ± 0.12	<.001
MTR (%)	38.6 ± 1.0	36.8 ± 1.1	.001
MD1k ($\times 10^{-3}$mm^2/s)	0.78 ± 0.02	0.83 ± 0.07	.008
MD3k ($\times 10^{-3}$mm^2/s)	0.65 ± 0.01	0.63 ± 0.03	.04

Note:—GM indicates gray matter; MD1k, mean diffusivity (b=1000 s/mm^2); MD3k, mean diffusivity (b=3000 s/mm^2); NS, not significant ($p \geq 0.1$); tv, modulated tissue segment fractional volume. Values are mean ± SD over subject group of the individual ROI means.

[a] WM is reported here because the SPM8 segmentation routine classifies the thalamus as a predominantly WM structure.

[b] *P* values are reported for the Mann-Whitney *U* test.

group.[8] The explanation for the prominent cognitive features of memory loss and frontal executive dysfunction in this patient group[32] is more complex.

Although the effect size maps (Fig 2) demonstrated some percentage difference in the mesial temporal lobes and prefrontal cortices, these volume losses were less marked compared with those in the cortical areas described above and did not prove to be statistically significant on VBM. Some of the memory and executive deficits seen in patients with *6-OPRI* mutations could be explained by subcortical pathologic changes affecting the cortical circuits involved in these cognitive functions. This finding would be supported by the subcortical gray matter volume loss seen in the caudate nuclei and putamina, as well as the MD and MTR changes in the posteromedial thalami.

Thalamic and striatal involvement is well established in all forms of human prion disease.[33] The putamen and caudate nuclei receive input from diverse cortical areas, including the prefrontal and limbic structures with nonmotor output from the striatum projecting, via the mediodorsal and ventrolateral thalamic nuclei, to the dorsolateral prefrontal cortex, lateral orbitofrontal cortex, and the anterior cingulate.[34]

Voxel-Based Analyses of MTR and MD

The MTR-VBA and MD-VBA did not show significant change in the basal ganglia; however, they demonstrated significant MTR reduction and significant MD increase in the posteromedial thalamus (not detected by VBM), cortical gray matter areas corresponding to those displaying VBM changes, and also in adjacent subcortical WM where no significant volume changes were detected. This finding suggests that MTR and MD data are a useful complement to T1-weighted structural data and are potentially more sensitive to subcortical WM and thalamic changes in prion diseases.

MTR-VBA

Our MTR findings are consistent with a previous study in which decreases in whole-brain and whole—gray matter segment MTR compared with controls were observed in patients with symptomatic prion disease, correlating with disease severity.[13] An association between decreased postmortem gray matter MTR and increased spongiosis was also seen in that study. One possible explanation for the differences in regional distribution of changes shown by MTR-VBA and VBM here is the potential of MTR to reflect microstructural pathologic changes (such as spongiosis), occurring before or independent of macroscopic volume loss.

MD-VBA

Our findings of increased cerebral MD in patients with the *6-OPRI* mutation have been reported in patients with IPD,[11,35] specifically in the cerebellar cortex in patients with the *E200K* mutation[18] and in the thalamus in variant Creutzfeldt-Jakob disease,[36,37] thought to reflect increased gliosis.[35,36] Opposite findings of decreased MD have been reported in sporadic Creutzfeldt-Jakob disease and in patients with the *E200K* mutation, specifically within the basal ganglia and thalamus,[11,14] thought to reflect spongiform change. A relationship between macroscopic atrophy and microscopic changes reflected in increased MD may be expected; in other neurodegenerative disorders, whole-brain or regional MD values usually increase in association with brain atrophy.[38,39] This increase in diffusivity has been associated with loss of neuronal cell bodies, synapses, and dendrites, causing an expansion of the extracellular space where water diffusivity is fastest.[40] Also, in prion diseases, this increase in diffusivity could reflect areas where neuronal loss and gliosis are becoming dominant over spongiform change but is too subtle to be detected by VBM.

High b-value DWI, relatively more sensitive to slowly diffusing tissue water components,[41] provided greater pathologic sensitivity for spongiform change than conventional b-value DWI in a previous study of sporadic Creutzfeldt-Jakob disease[11] and in patients with IPD who have the *E200K* mutation frequently mimicking the sporadic Creutzfeldt-Jakob disease phenotype.[14]

However, in the former study[11], high b-value DWI was not more sensitive than conventional b-value DWI in the detection of increased ADC values in the pulvinar nucleus in patients with variant Creutzfeldt-Jakob disease, thought to have histopathologic features of gliosis. It is likely that in the context of gliosis and neuronal loss, fast diffusion components dominate the mean diffusivity so that high b-value DWI is less sensitive, as was observed in our study.

ROI Analysis

Although MD-VBA and MTR-VBA did not reveal significant changes in the basal ganglia, significant ROI MD increases and MTR decreases were seen in the thalamus, putamen, and caudate in the *6-OPRI* subgroup relative to control participants. Voxel-based analyses may not provide a complete substitute but, rather, a complement to ROI analysis, the latter potentially avoiding smoothing across interregional or tissue boundaries. Cross-boundary smoothing in VBA complicates interpretation and can either reduce or increase statistical power, depending on whether the greatest underlying changes respect the observable tissue boundaries. Intergroup differences revealed on VBA and VBM may identify pathologically specific affected regions. These differences may then be more sensitively investigated on a subject-by-subject basis by ROI analysis, which may provide the most straightforward and interpretable way to monitor disease progression.

Study Limitations

Patients with the *6-OPRI* mutation were the largest mutation subgroup to undergo MR imaging scanning in the PRION-1 trial, and our current study represents the largest group of such patients for which consistent multiparameter MR imaging measurements are available. Nevertheless, given the relatively small group size, our analysis should be considered preliminary.

Some types of IPD (*E200K*, *V201I*) have clinical and radiologic features similar to sporadic Creutzfeldt-Jakob disease,[42] but apart from patients carrying the *P102L* mutation,[9] the imaging features of other mutations are not well described in the literature. A comparison of *6-OPRI* MR imaging findings with those from other IPD mutations would be particularly informative. Although we had access to another small set ($n = 8$) of patients with IPD who had other mutations, the subgroups were too small ($n = 4$, $n = 1$, $n = 1$, $n = 1$, $n = 1$) to achieve statistical power sufficient to provide robust conclusion on differences and similarities among mutations. Future trials enrolling larger patient numbers will be necessary for this type of analysis.

Our data suggest that in a number of brain regions, MTR and MD appear more sensitive to pathologic changes than the tissue-volume data inferred from the T1-weighted acquisition. A future study with a larger dataset may confirm this observation by seeking significant changes after adjusting for local atrophy by using voxelwise covariates (also known as biologic parametric mapping).[43,44] Furthermore, for our current data we underline that the specific sensitivities (and statistical power) of the individual voxel-based analyses also depend on the acquisition signal-to-noise ratios in the respective protocols (eg, determined by specific sequence parameters, including nominal voxel sizes). We used the standard acquisition parameters optimized for each method at our institution; our current study was not designed to systematically compare protocols with matched signal-to-noise ratios.

Although the voxel-based analyses were performed on normalized images with a nominal isotropic resolution (1.5 mm),[3] the DWI and MTR source data were acquired with a larger section thickness (5 mm) compared with the nominal 1.5-mm partition of the 3D structural images. Partial-volume averaging from CSF at the brain surface may thus be partly responsible for the larger clusters detected proximal to the brain-CSF interfaces on MTR-VBA and MD-VBA. With this problem in mind, we took care to ensure that CSF contamination did not influence the manually drawn ROIs.

CONCLUSIONS

Our study is the first multiparameter voxel-based analysis of cerebral atrophy and microstructural changes in the *6-OPRI* IPD mutation by using quantitative MR imaging. With VBM, we demonstrated regionally specific volume loss corresponding anatomically to clinical symptoms and providing an anatomic basis for the memory and executive function deficits seen clinically. We also showed that VBA of MTR and MD can detect microstructural changes in anatomic regions that do not demonstrate volume loss on VBM. This finding is likely to reflect a diverse anatomic distribution of histopathologic change driven by varying pathophysiologic processes. Combining regional measures from different but complementary MR imaging modalities can identify brain regions preferentially involved in the pathophysiology of prion disease and may provide markers of value in monitoring future therapies. Comparison of our data on patients with the *6-OPRI* mutation with existing literature suggests that the distribution of structural and microstructural changes presented here is specific to this particular IPD mutation.

ACKNOWLEDGMENTS

We thank all patients and relatives for taking part in this study, present and past staff of the National Prion Clinic, the radiography staff from the National Hospital for Neurology and Neurosurgery, Prof. Gareth Barker for assistance with implementing the magnetization transfer sequence, and Ray Young for the figures. We thank neurologic and other colleagues throughout the United Kingdom for referral of patients.

Disclosures: Gerard Ridgway—*RELATED: Grant:* Wellcome Trust,* Comments: The Wellcome Trust Centre for Neuroimaging is supported by core funding from the Wellcome Trust, grant no. 079866/Z/06/Z; *UNRELATED: Payment for Lectures (including service on speaker bureaus):* University of Zurich, Comments: Honoraria paid for teaching on the Zurich SPM course. Tarek Yousry—*RELATED: Grant:* UCL-UCLH Biomedical Research Centre;* *UNRELATED: Board Membership:* Editorial Board of *European Radiology*, Comments: No payments were received; *Consultancy:* GlaxoSmithKline,* Biogen Idec,* Novartis; *Grants/Grants Pending:* Medical Research Council,* MS Society of Great Britain and Northern Ireland,* PSP Association,* Stroke Association,* British Heart Foundation,* Wellcome Trust;* *Payment for Development of Educational Presentations:* ESOR, King Abdullah Medical City. John Collinge—*RELATED: Grant:* Medical Research Council,* Department of Health;* *UNRELATED: Board Membership:* D-Gen Limited, Comments: Director and Shareholder Academic spinout company in the field of prion disease (no salary). Hans Rolf Jäger—*UNRELATED: Grants/Grants Pending:* Stroke Association,* British Heart Foundation,* Radiological Research Trust* NIHR.* John Thornton—*UNRELATED: Grants/Grants Pending:* GlaxoSmithKline.* (**Money paid to institution.*)

REFERENCES

1. Collinge J. **Prion diseases.** In: Ledingham JGG, Warrell DA, eds. *Concise Oxford Textbook of Medicine.* New York: Oxford University Press, 2000;1307–11
2. Collinge J, Rossor M. **A new variant of prion disease.** *Lancet* 1996;347:916–17
3. Hill AF, Collinge J. **Subclinical prion infection in humans and animals.** *Br Med Bull* 2003;66:161–70
4. Llewelyn CA, Hewitt PE, Knight RS, et al. **Possible transmission of variant Creutzfeldt-Jakob disease by blood transfusion.** *Lancet* 2004;363:417–21

5. Wroe SJ, Pal S, Siddique D, et al. **Clinical presentation and pre-mortem diagnosis of variant Creutzfeldt-Jakob disease associated with blood transfusion: a case report.** *Lancet* 2006;368:2061–67
6. Mead S. **Prion disease genetics**. *Eur J Hum Genet* 2006;14:273–81
7. Kaski DN, Pennington C, Beck J, et al. **Inherited prion disease with 4-octapeptide repeat insertion: disease requires the interaction of multiple genetic risk factors**. *Brain* 2011;134:1829–38
8. Mead S, Poulter M, Beck J, et al. **Inherited prion disease with six octapeptide repeat insertional mutation–molecular analysis of phenotypic heterogeneity.** *Brain* 2006;129:2297–317
9. Alner K, Hyare H, Mead S, et al. **Distinct neuropsychological profiles correspond to distribution of cortical thinning in inherited prion disease caused by insertional mutation.** *J Neurol Neurosurg Psychiatry* 2012;83:109–14
10. Fox NC, Freeborough PA, Mekkaoui KF, et al. **Cerebral and cerebellar atrophy on serial magnetic resonance imaging in an initially symptom free subject at risk of familial prion disease.** *BMJ* 1997;315:856–57
11. Hyare H, Thornton J, Stevens J, et al. **High-b-value diffusion MR imaging and basal nuclei apparent diffusion coefficient measurements in variant and sporadic Creutzfeldt-Jakob disease.** *AJNR Am J Neuroradiol* 2010;31:521–26
12. Hyare H, Wroe S, Siddique D, et al. **Brain-water diffusion coefficients reflect the severity of inherited prion disease.** *Neurology* 2010;74:658–65
13. Siddique D, Hyare H, Wroe S, et al. **Magnetization transfer ratio may be a surrogate of spongiform change in human prion diseases.** *Brain* 2010;133:3058–68
14. Lee H, Hoffman C, Kingsley PB, et al. **Enhanced detection of diffusion reductions in Creutzfeldt-Jakob disease at a higher B factor.** *AJNR Am J Neuroradiol* 2010;31:49–54
15. Ashburner J, Friston KJ. **Voxel-based morphometry–the methods.** *Neuroimage* 2000;11:805–21
16. Lee H, Rosenmann H, Chapman J, et al. **Thalamo-striatal diffusion reductions precede disease onset in prion mutation carriers.** *Brain* 2009;132:2680–87
17. Lee H, Cohen OS, Rosenmann H, et al. **Cerebral white matter disruption in Creutzfeldt-Jakob disease.** *AJNR Am J Neuroradiol* 2012;33:1945–50
18. Cohen OS, Hoffmann C, Lee H, et al. **MRI detection of the cerebellar syndrome in Creutzfeldt-Jacob disease.** *Cerebellum* 2009;8:373–81
19. Collinge J, Gorham M, Hudson F, et al. **Safety and efficacy of quinacrine in human prion disease (PRION-1 study): a patient-preference trial.** *Lancet Neurol* 2009;8:334–44
20. Folstein MF, Folstein SE, McHugh PR. **"Mini-mental state". A practical method for grading the cognitive state of patients for the clinician.** *J Psychiatr Res* 1975;12:189–98
21. Hughes CP, Berg L, Danziger WL, et al. **A new clinical scale for the staging of dementia.** *Br J Psychiatry* 1982;140:566–72
22. Stejskal EO, Tanner JE. **Spin diffusion measurements: spin echoes in the presence of a time-dependent field gradient.** *J Chem Phys* 1965;42:288–92
23. Barker GJ, Schreiber WG, Gass A, et al. **A standardised method for measuring magnetisation transfer ratio on MR imagers from different manufacturers–the EuroMT sequence.** *MAGMA* 2005;18:76–80
24. Barker GJ, Tofts PS, Gass A. **An interleaved sequence for accurate and reproducible clinical measurement of magnetization transfer ratio.** *Magn Reson Imaging* 1996;14:403–11
25. Ashburner J, Friston KJ. **Unified segmentation.** *Neuroimage* 2005;26:839–51
26. Ashburner J. **A fast diffeomorphic image registration algorithm.** *Neuroimage* 2007;38:95–113
27. Mechelli A, Price CJ, Friston KJ, et al. **Voxel-based morphometry of the human brain: methods and applications.** *Curr Med Imag Rev* 2005;1:105–13
28. Ourselin S, Roche A, Subsol G, et al. **Reconstructing a 3D structure from serial histological sections.** *Image Vis Comput* 2001;19:25–31
29. Ourselin S, Stefanescu, R, Pennec X. Robust registration of multimodal images: Towards real-time clinical applications. In: Proceedings of Medical Image Computing and Computer-Assisted Intervention (MICCAI), Tokyo, Japan, September 25–28, 2002:140–47
30. Ridgway GR, Omar R, Ourselin S, et al. **Issues with threshold masking in voxel-based morphometry of atrophied brains.** *Neuroimage* 2009;44:99–111
31. Arata H, Takashima H, Hirano R, et al. **Early clinical signs and imaging findings in Gerstmann-Sträussler-Scheinker syndrome (Pro102Leu).** *Neurology* 2006;66:1672–78
32. Cordery RJ, Alner K, Cipolotti L, et al. **The neuropsychology of variant CJD: a comparative study with inherited and sporadic forms of prion disease.** *J Neurol Neurosurg Psychiatry* 2005;76:330–36
33. Aguzzi A, Weissmann C. **Prion diseases**. *Haemophilia* 1998;4:619–27
34. Middleton FA, Strick PL. **Basal-ganglia 'projections' to the prefrontal cortex of the primate.** *Cereb Cortex* 2002;12:926–35
35. Haik S, Galanaud D, Linguraru MG, et al. **In vivo detection of thalamic gliosis: a pathoradiologic demonstration in familial fatal insomnia.** *Arch Neurol* 2008;65:545–49
36. Oppenheim C, Brandel JP, Hauw JJ, et al. **MRI and the second French case of vCJD.** *Lancet* 2000;356:253–54
37. Waldman AD, Jarman P, Merry RT. **Rapid echoplanar diffusion imaging in a case of variant Creutzfeldt-Jakob disease; where speed is of the essence.** *Neuroradiology* 2003;45:528–31
38. Kantarci K, Jack CR Jr, Xu YC, et al. **Mild cognitive impairment and Alzheimer disease: regional diffusivity of water.** *Radiology* 2001;219:101–07
39. Mascalchi M, Lolli F, Della Nave R, et al. **Huntington disease: volumetric, diffusion-weighted, and magnetization transfer MR imaging of brain.** *Radiology* 2004;232:867–73
40. Kantarci K, Petersen C, Boeve BF, et al. **DWI predicts future progression to Alzheimer disease in amnestic mild cognitive impairment.** *Neurology* 2006;64:902–04
41. Niendorf T, Dijkhuizen RM, Norris DG, et al. **Biexponential diffusion attenuation in various states of brain tissue: implications for diffusion-weighted imaging.** *Magn Reson Med* 1996;36:847–57
42. Breithaupt M, Romero C, Kallenberg K, et al. **Magnetic resonance imaging in E200K and V210I mutations of the prion protein gene**. *Alzheimer Dis Assoc Disord* 2013;27:87–90
43. Casanova R, Srikanth R, Baer A, et al. **Biological parametric mapping: A statistical toolbox for multimodality brain image analysis.** *Neuroimage* 2007;34:137–43
44. Oakes TR, Fox AS, Johnstone T, et al. **Integrating VBM into the general linear model with voxelwise anatomical covariates.** *Neuroimage* 2007;34:500–08